CrossMark

SMOS sea ice product: Operational application and validation in the Barents Sea marginal ice zone

Lars Kaleschke [a,*], Xiangshan Tian-Kunze [a], Nina Maaß [a], Alexander Beitsch [a,b], Andreas Wernecke [a], Maciej Miernecki [a], Gerd Müller [c], Björn H. Fock [c,d], Andrea M.U. Gierisch [c,e], K. Heinke Schlünzen [c], Thomas Pohlmann [a], Mikhail Dobrynin [a], Stefan Hendricks [f], Jölund Asseng [f], Rüdiger Gerdes [f,h], Peter Jochmann [g], Nils Reimer [g], Jürgen Holfort [i], Christian Melsheimer [j], Georg Heygster [j], Gunnar Spreen [k,j], Sebastian Gerland [k], Jennifer King [k], Niels Skou [l], Sten Schmidl Søbjærg [l], Christian Haas [m], Friedrich Richter [n], Tânia Casal [n]

[a] Institute of Oceanography, University of Hamburg, Germany
[b] Now at Max Planck Institute for Meteorology, Hamburg, Germany
[c] Meteorological Institute, University of Hamburg, Germany
[d] Now at Met Office, Exeter, UK
[e] Now at Finnish Meteorological Institute, Helsinki, Finland
[f] Alfred-Wegener-Institut Helmholtz-Zentrum für Polar- und Meeresforschung, Bremerhaven, Germany
[g] Hamburgische Schiffbau-Versuchsanstalt GmbH, Hamburg, Germany
[h] Jacobs University, Bremen, Germany
[i] Bundesamt für Seeschifffahrt und Hydrographie, Germany
[j] Institute of Environmental Physics, University of Bremen, Germany
[k] Norwegian Polar Institute, Norway
[l] DTU Space, Denmark
[m] York University, Toronto, Canada
[n] ESTEC, ESA, Noordwijk, Netherlands

ABSTRACT

Brightness temperatures at 1.4 GHz (L-band) measured by the Soil Moisture and Ocean Salinity (SMOS) Mission have been used to derive the thickness of sea ice. The retrieval method is applicable only for relatively thin ice and not during the melting period. Hitherto, the availability of ground truth sea ice thickness measurements for validation of SMOS sea ice products was mainly limited to relatively thick ice. The situation has improved with an extensive field campaign in the Barents Sea during an anomalous ice edge retreat and subsequent freeze-up event in March 2014. A sea ice forecast system for ship route optimisation has been developed and was tested during this field campaign with the ice-strengthened research vessel RV Lance. The ship cruise was complemented with coordinated measurements from a helicopter and the research aircraft Polar 5. Sea ice thickness was measured using an electromagnetic induction (EM) system from the bow of RV Lance and another EM-system towed below the helicopter. Polar 5 was equipped among others with the L-band radiometer EMIRAD-2. The experiment yielded a comprehensive data set allowing the evaluation of the operational forecast and route optimisation system as well as the SMOS-derived sea ice thickness product that has been used for the initialization of the forecasts. Two different SMOS sea ice thickness products reproduce the main spatial patterns of the ground truth measurements while the main difference being an underestimation of thick deformed ice. Ice thicknesses derived from the surface elevation measured by an airborne laser scanner and from simultaneous EMIRAD-2 brightness temperatures correlate well up to 1.5 m which is more than the previously anticipated maximal SMOS retrieval thickness.

© 2016 Elsevier Inc. All rights reserved.

1. Introduction

The recent strong decline of Arctic sea ice not only substantiates concerns about human-generated global warming and associated weather extremes but also raises interest in Arctic shipping and the need for operational sea ice forecast system. Sea ice thickness is one of the key parameters needed both for the initialisation and for the validation of forecast models (Day, Hawkins, & Tietsche, 2014; Yang et al., 2014). It can be derived from the freeboard conversion using altimetry (e.g. from CryoSat-2) or from microwave radiometry at low frequencies (Laxon et al., 2013; Ricker, Hendricks, Helm, Skourup, & Davidson,

2014; Kwok & Cunningham, 2015; Kaleschke, Tian-Kunze, Maaß, Mäkynen, & Drusch, 2012). One major advantage of microwave radiometry is the wide swath coverage that allows daily sampling of large parts of the Arctic. The two retrieval techniques are complementary because the freeboard method has a large relative uncertainty for thin ice while the radiometric approach is not sensitive for ice thicker than the penetration depth of the electromagnetic waves in the ice medium. This maximum ice thickness depends on the liquid brine concentration in the ice and thus on the ice salinity and temperature. At the SMOS frequency of 1.4 GHz the maximum thickness was estimated to be less than half a meter for homogenous Arctic level ice (Kaleschke, Maass, Haas, Heygster, & Tonboe, 2010). The SMOS mission was originally proposed for estimating surface soil moisture and sea surface salinity but significant research progresses were also expected over the cryosphere (Kerr et al., 2001).

An algorithm developed at the University of Hamburg (UH) is based on a combined thermodynamic and radiative transfer model which accounts for variations of ice temperature and ice salinity (Tian-Kunze et al., 2014; Mecklenburg et al., 2016). The UH algorithm further accounts for an assumed lognormal shape of the statistical thickness distribution which results in a two to threefold maximum mean thickness up to 1.5 m. An empirical algorithm developed at the University of Bremen (UB) is based on training data obtained from ice growth models (Huntemann et al., 2014). The validation of the UB and UH SMOS sea ice thickness data products so far was limited to sparsely available ground truth and considerable uncertainties remained (Kaleschke et al., 2013; Maaß et al., 2015). A main limitation is the applicability of the SMOS sea ice thickness retrieval methods to cold seasons and excludes its use during melting periods.

A dedicated field campaign was conducted in the Barents Sea in March 2014 and gained a substantial amount of new validation data over thin ice. The new validation data comprises measurements from a helicopter based on RV Lance and the research aircraft Polar 5 operated from Longyearbyen airport, Spitsbergen. Sea ice thickness was measured using an electromagnetic induction (EM) system from the bow of RV Lance (Haas, 1998) and another EM-system towed below the helicopter (HEM) (Haas, Lobach, Hendricks, Rabenstein, & Pfaffling, 2009). Polar 5 was equipped among others with a laser scanner (ALS) used to determine sea ice freeboard and the radiometer EMIRAD-2 that measured the fully-polarimetric 1.4 GHz brightness temperature at nadir and tilted at 45°. This paper will provide an overview of the campaign and will present first results of the validation of SMOS sea ice thickness products. We thereby assume the ship-based and airborne measurements as "ground validation data" to assess the quality of the SMOS sea ice thickness retrievals. Furthermore, we show an example application of ship route optimization based on the results of a sea ice model forecast initialized with SMOS and AMSR2 data.

One important goal of the RV Lance cruise was to test this newly developed ice route optimization system which predicts the most efficient route in terms of safety and timesaving for ships navigating in ice infested Arctic waters. The system is based on a high resolving coupled Atmosphere–Sea Ice–Ocean model predicting ice thickness and concentration. These data are used by a software calculating time optimized routing alternatives. Because predicted data are used the ship's guidance is not only based on the ice situation observed in advance of the cruise but also on changes to be expected during the cruise. A main goal of the cruise was to validate the ice route optimization system's performance by passing through the proposed ice routes while assessing the relation of ship's performance and ice conditions, by comparing predicted travel duration with achieved duration, and, in some cases, by trying out what happens when a proposed redirection was ignored. No in-situ ice and snow measurements have been performed because they would have interrupted the test of the ice route optimization system.

The paper is organized as follows. The following section describes the sea ice condition and the set-up of the field experiment in the Barents Sea. The measurements and choice of parameters used to derive

the sea ice thickness retrieval are summarized in Sections 3 and 4. The application of the SMOS data for sea ice forecast and ship route optimization is described in Section 6. In Section 5 the results of the comparisons are presented and discussed. The last section concludes the paper.

The aim of this paper is to describe the state and performance of SMOS sea ice retrieval algorithms based on the SMOS Level 1C data version V5.05 available during the experiment in March 2014. Improvements based on experience with the validation data acquired during this and other campaigns and with more recent SMOS data versions as well as the combination of SMOS and CryoSat2 (Kaleschke et al., 2015) are subject for subsequent papers.

2. Physical conditions and experimental set-up

The main experimental area between Edgeøya and Kong Karls Land in the east of Svalbard belongs to the Barents Sea which in most years features only a seasonal ice cover despite its high latitude (Smedsrud et al., 2013). The boundary between the relatively warm water brought through the Norwegian Atlantic Current and the cold East Spitsbergen Current defines the oceanic Polar Front (Pavlova, Pavlov, & Gerland, 2014). The climatological minimum winter sea ice extent was given as the latitude of 77°N (Sandven, Johannessen, Miles, Pettersson, & Kloster, 1999). However, the physical conditions between the second half of January to the first half of March 2014 deviated strongly from the climatology. The air temperature measured at Hopen Island meteorological station was on average 9 °C to 12 °C above the climatological value as defined for the period of 1961 to 1990 (Strübing & Schwarz, 2014). Southerly winds pushed the sea ice at the coast between Barentsøya and Nordaustlandet and only a relatively small strip of compacted ice remained at the beginning of the experiment (Fig. 2).

A comparison of historical hydrographic data over the years 1923–2011 with 33 CTD-measurements (Conductivity, Temperature, Depth) conducted during the RV Lance cruise revealed an anomalously northern location of the Polar Front in March 2014 (Dobrynin & Pohlmann, 2015). Significantly warmer (by up to 3.8 °C) and saltier (by up to 2.49 g/kg) conditions were observed in 2014 for nine out of ten stations in a point by point comparison with historical stations in 1983 and 1986. The surface salinity was measured covering the Atlantic and Arctic water masses on both sides of the Polar Front: in the Storfjorden Trench (approximately 35.05 g/kg) and in the Olga Basin south of Kongsøya (approximately 34.60 g/kg). During the main experimental phase between March 16 and March 27 the air temperature at Hopen was about 5 °C above the climatological mean. The near-surface air temperatures varied between −10 °C to −15 °C and caused new ice growth in the area of investigation. The anomalous ice retreat together with the subsequent refreezing created the perfect conditions to acquire sea ice thickness validation data over thin ice.

An array of 15 ice drift buoys was deployed from an aircraft before the ship cruise to measure the ice movement. The drift trajectories from the buoys are useful to determine the origin of the ice and help to determine if thickness changes are caused by ice dynamics or ice growth and melting (Figs. 2 and 3). In addition to 11 Cosmos-Skymed and 8 Radarsat scenes 83 TerraSAR-X images have been acquired in the new experimental 6-beam wide-swath mode to support the interpretation of the field data and to validate ice motion algorithms.

3. Sea ice thickness from electromagnetic induction

Electromagnetic induction (EM) measurements rely on the large contrast in electrical conductivity between sea ice and seawater. An electromagnetic field generated by a transmitter coil induces electrical eddy currents mainly in the seawater below the ice. A second receiver coil measures the secondary field produced by the eddy currents. The ratio of the secondary to the primary field depends on the height of the coils above the sea surface. Ice thickness can be calculated when

the distance of the instrument to the ice surface is known (Haas, 1998; Haas et al., 2009).

The distance to the snow or ice surface was measured by an ultrasonic sensor for the Geonics EM31 system installed at the bow of RV Lance and by a Riegl LD90-3 laser altimeter for the EM-Bird carried below the helicopter. The EM-Bird was built by Ferra Dynamics Inc., Ontario, Canada. Henceforth we will use the abbreviations SEM and HEM to distinguish between the shipborne and the helicopter EM systems, respectively.

The SEM was installed below an aluminium boom mounted like a bowsprit to reduce the influence of the ship hull and other conductive parts. It was lowered from the boom resulting in a distance to the ship hull of around 7 m with the distance to the water surface between 3 to 4 m (Figs. 1 and 4). The time resolution of the SEM was 2 Hz and the ice thickness measurement was complemented with 10 Hz-measurements of surface temperature by a radiation thermometer of type KT19, installed at the bow at the foremost point of the railing and looking downward along an angle of about 30°. With a beam width of 1° the resulting KT19 footprint had a diameter of about 1 m and was within the footprint of the SEM which had a diameter of about 5 m. Two calibrations of the SEM were performed, the first in Longyearbyen on March 14 and a second one within a small patch of open water in the sea ice on March 19. After that the SEM instrument was operated continuously and stable ice thickness results could be retrieved without any further correction. The accuracy and precision of the SEM thickness measurement was about 2 cm as estimated over thin nilas (Fig. 4) and the signal was remarkably stable — as seen by the accurate detection of zero levels in leads — for the 1800 km track (Fig. 5). The accuracy decreased in the presence of surface waves which were present in particular during the last southerly sections of the cruise on March 26 and thereafter.

The HEM system is operated at a height of approximately 15 m above the sea ice surface. With a nominal flying speed of 70 knots (36 m/s), the sea ice thickness is measured every 3 to 4 m within a footprint of about 50 m. In total eight HEM flights were performed as summarized in Table 1. The HEM data processing involves some manual steps to remove the instrument drift during the measurements and to define the zero ice thickness level. To avoid unrealistic data the processing routine automatically removes data outside minimum & maximum thresholds in laser height, and data that coincide with a change in heading (to avoid roll events on change of direction). Other small gaps in the data occur due to GPS dropout and to the laser failing over open water. The nominal uncertainty for a single ice thickness measurement is 10 cm for level ice while larger errors can occur for ridges (Haas et al., 2009). Both the SEM and the HEM measure the thickness of sea ice

Fig. 1. RV Lance during the field experiment in the Barents Sea, 24 March 2014. The EM system at the bow is visible by its red color. Photograph taken from Polar 5 aircraft by Stefan Hendricks.

plus snow. We note that the helicopter usually avoided flying over thin ice and open water for safety reasons while the ship mainly navigated through leads (Fig. 4).

4. Sea ice thickness from airborne laser scanner and L-band radiometer

One primary goal of the airborne field campaign was to obtain high resolution, polarized L-Band brightness temperatures at different incident angles together with independent sea ice thickness measurements for the validation of retrieval algorithms. The two primary independent data sources are the EM-bird flown from the helicopter and the ALS aboard the Polar 5. In this campaign only measurements from the latter instrument are truly co-incident and co-located with the L-Band radiometer EMIRAD-2. The combination of ALS and EMIRAD-2 data is thus suitable to assess the performance of the instruments and to verify the retrieval of thickness from 1.4 GHz brightness temperatures at high spatial resolution. Comparisons between ALS and SMOS ice thickness will be discussed in the next section.

The EMIRAD-2 L-band radiometer developed by DTU-Space is a fully polarimetric system with advanced RFI detection features (Sobjaerg, Kristensen, Balling, & Skou, 2013). Two Potter horn antennas — one nadir pointing, one side looking at 45° incidence angle measure the radiation from the surface with a footprint of approximately 250 m at 300 m flight altitude. The receiver has a sensitivity of 0.1 K for 1 s integration time. Internal calibration every 8 to 16 min maintains a stability of better than 0.1 K. External calibration with liquid Nitrogen gives estimates of the uncertainty associated with the cables connecting the antenna to the receiver below 0.5 K of equivalent noise temperature. During all flight operations navigation data are collected and used to transform the polarimetric brightness temperature into the Earth reference frame (Hendricks et al., 2014).

The EMIRAD-2 data have been screened by evaluating kurtosis, polarimetric, and brightness temperature anomalies and revealed up to 30% radio frequency interference (RFI) contamination. When subtracting the mean value of the RFI-flagged data from the mean value of the full data a difference of typically a few K is present for side looking horn and typically 10 K for the nadir looking horn. Especially for the last flight on March 26, a difference of 25 K between raw and cleaned data is observed for the nadir looking horn. Data analysis further revealed a 20 K offset relative to the nadir vertical channel caused by a continuous wave signal from the camera that was mounted at the airplane to obtain visual images. This contamination could not be detected by the RFI filters but the analysis concludes a purely additive characteristic and allowed a bias correction (Hendricks et al., 2014). In the following we use an RFI-cleaned and bias-corrected data set which was validated using aircraft wing wags and nose wags over open ocean (Hendricks et al., 2014).

A Riegl VQ-580 laser scanner (ALS) used on the Polar 5 operates in near infrared with an accuracy and precision of 25 mm over snow and ice. The linear across-track scans are performed in the range of 30° to −30° with a pulse repetition frequency of 50 kHz leading to a horizontal sampling resolution of 30 cm at 60 m altitude. A calibration of the instrument mounting position and orientation in the aircraft reference frame was done using a fixed ground target, namely the airport buildings in Longyearbyen. The determination of the ellipsoidal (WGS84) surface heights from the laser range data and the aircraft altitude and instrument mounting position and orientation was performed according to Helm et al. (2006). Finally, the surface height was referenced to the local sea level by manual classification of tie points in leads.

The ALS freeboard data are resampled to 1 s and to 1 min by taking the arithmetic mean value. To estimate the ice thickness from the freeboard one has to make some assumptions about the density of ice and snow and the snow thickness. While the snow depth on the sea ice was not measured in situ, continuous visual observations from Lance were done. From these observations as well as from imagery from a
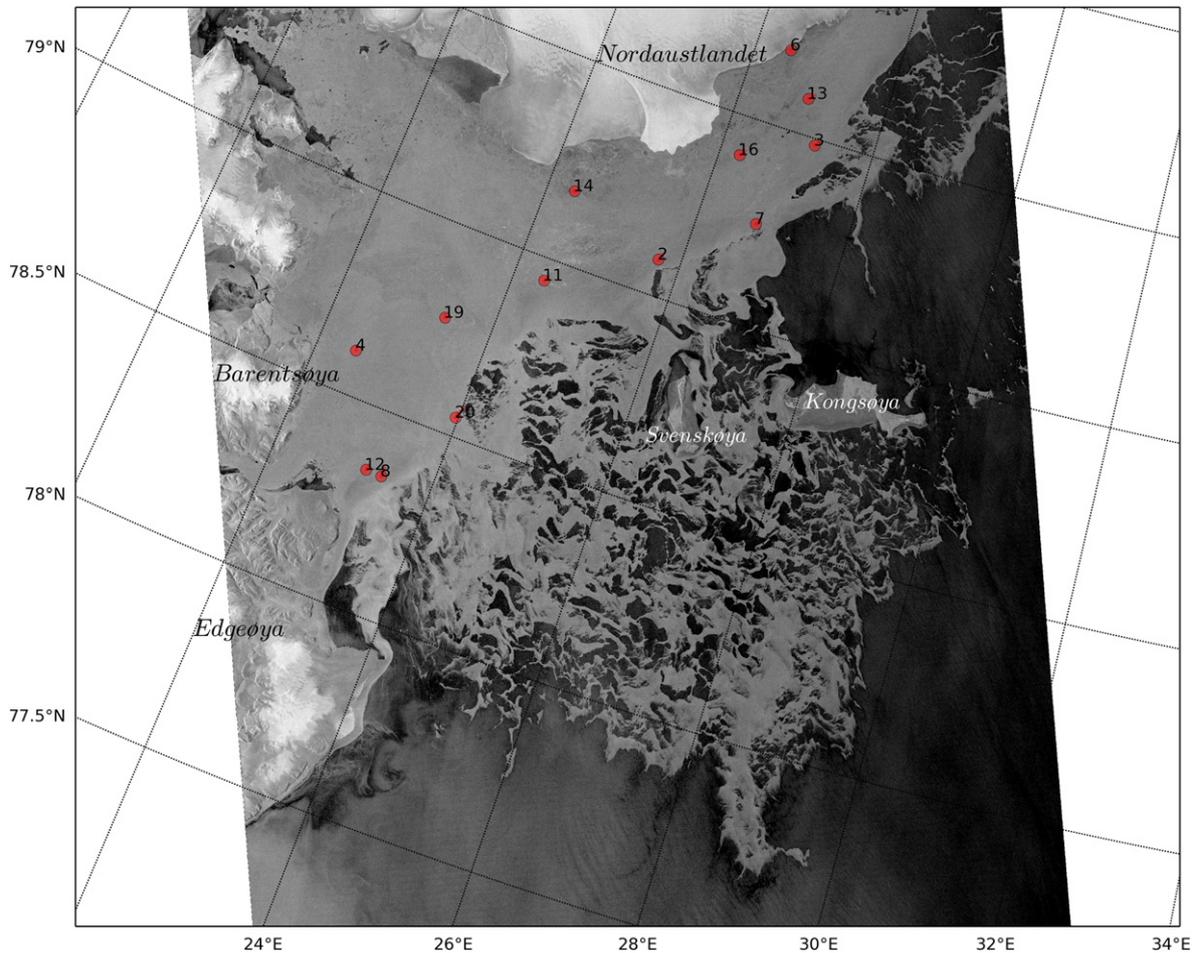
Fig. 2. Sea ice condition at the beginning of the field experiment. The TerraSAR-X wide swath frames (HH polarization) were taken on March 8 at 14:50. The positions of ice drift buoys are indicated for March 10 at 14:00.

camera at the bow of the ship, the snow cover of the ice near the ship can be estimated to be a few centimeters whenever the ship was in thin ice (when the thickness measured by the SEM is between about 0 and 20 cm). Only very thin ice like freshly frozen leads was snow-free. Snow depths near 10 cm were only observed occasionally when the ship was navigating through thicker floes or ridges (SEM reading about 1 m). In addition, snow depth on the sea ice was retrieved from AMSR2 (UB product, based on the algorithm by (Markus and Cavalieri (2013)) with a resolution of about 15 km. Only in the region Northeast of Egdeøya (where ice thickness in Fig. 7 exceeds 1 m), the retrieved snow depth reaches 20 cm while in all other areas, the retrieved snow depths are generally between 0 and 5 cm throughout the cruise. Therefore, it is justified to use a simple parameterization $h_s = 0.1 \cdot h_i$, with the snow thickness h_s and ice thickness h_i (Yu & Rothrock, 1996; Mäkynen, Cheng, & Similä, 2013).

We assume a snow density of 300 kg/m^3 (Warren et al., 1999), a typical density of first year ice as 917 kg/m^3 (Ricker et al., 2014), and seawater as 1027 kg/m^3. The resulting factor of 5.6 is used to estimate the ice thickness from the ALS freeboard measurement. The assumption of a snow-free ice surface results in a conversion factor of about 9. The difference of both calculations can be seen as a first rough error estimate of the ALS thickness retrieval: with the assumption of a snow free ice surface we obtain a maximum observed sea ice thickness of about 4 m (1 min average). It reduces to about 2 m with the assumption of the snow thickness as 10% of the ice thickness.

Fig. 3 shows the tracks flown on 24 March 2014. Fig. 6 depicts the east-west profile from the position 78.0°N, 29.4°E to 78.25°N, 23.0°E (155 km length). This case includes a strong gradient from thin

newly-formed ice to thick deformed ice. The data of the other Polar 5 tracks on March 24 look very similar and are therefore not shown. The mean thickness derived from ALS for the track shown in Fig. 6 is 0.8 m and 1.3 m for the assumption of $h_s = 0.1 \cdot h_i$ and for the snow-free surface, respectively. The corresponding ice thickness retrieved from EMIRAD-2 using the operational SMOS algorithm described in Tian-Kunze et al. (2014) is 1 m. The correlation coefficient between ALS and EMIRAD-2 ice thickness is $R \approx 0.9$ and the RMSD is 0.3 m for the overall track ($N = 105$ data points).

When only the first and last 15 min are considered (thus omitting the transition zone between thin and thick ice) slightly reduced correlations of $R \approx 0.7$ ($N = 45$) are obtained while the RMSD remains similar. The mean values of both 15 min sections shown in Fig. 6 demonstrate that the thin and thick ice regimes can be well distinguished. The EMIRAD-2 thickness is greater than the ALS thickness estimate for the snow-covered and lower compared to the snow-free assumption. The brightness temperatures from SMOS are about 10 K lower compared to the EMIRAD-2 measurements but the gradient is well captured with however much coarser resolution. The differences can be explained with the coarse resolution of SMOS 100 × 100 bigger than the EMIRAD-2 footprint. The footprints of the indivdual SMOS measurements that are averaged into the 12.5 km grid have resolutions of about 35–40 km. EMIRAD-2 samples only a small fraction and is not representative for the SMOS measurement area. Moreover, we can not rule out problems with the bias correction and problems due to self-reflection of the aircraft. Special care was taken to avoid potential sun glint but some uncertainty still remains. A comparison of low-level and high-level flights in opposite directions showed no systematic
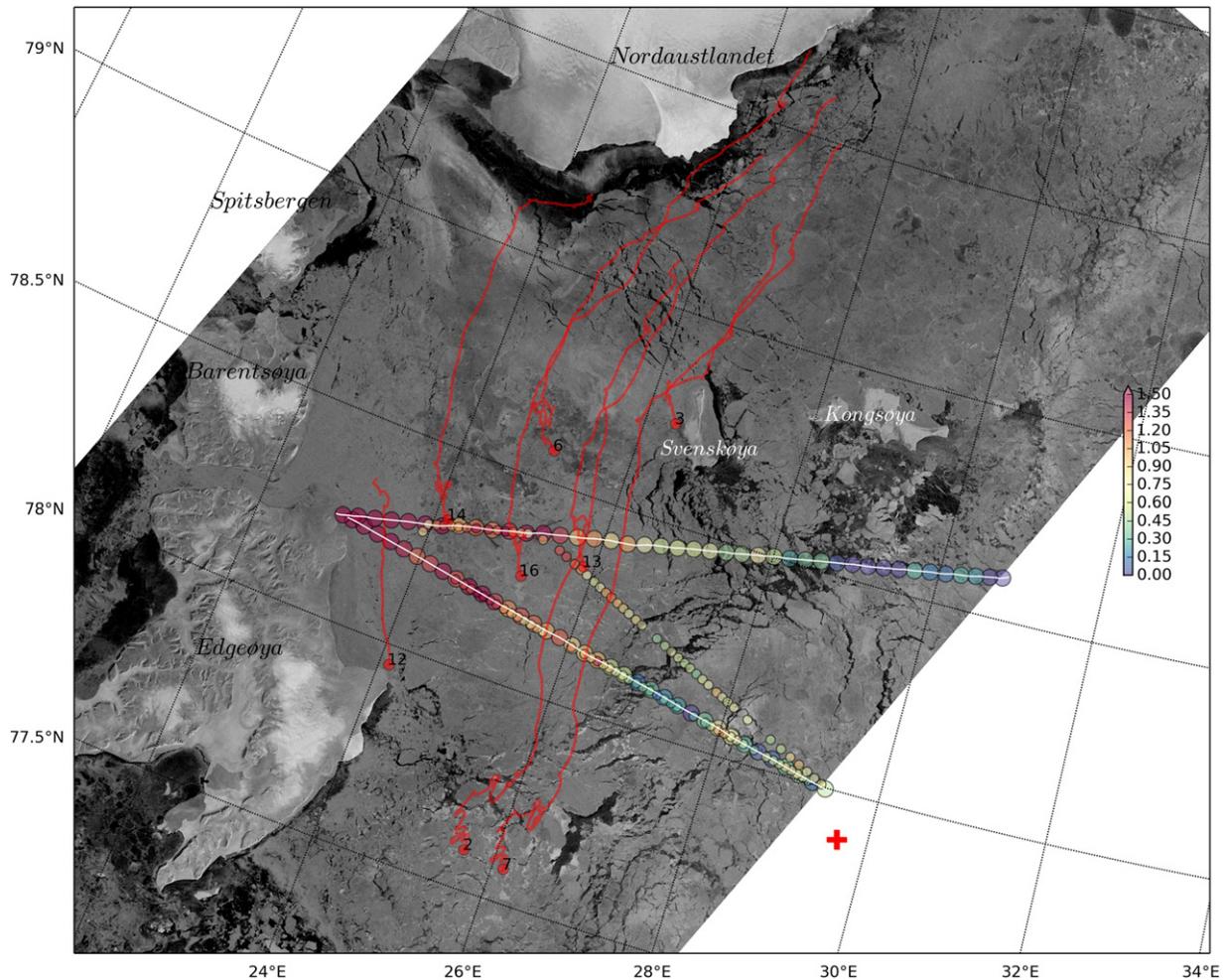
Fig. 3. Sea ice condition during the field experiment on March 24. The TerraSAR-X wide swath frames were taken at 05:36. The positions and trajectories of ice drift buoys are indicated with red circles and lines. Only those buoys are selected that transmitted their positions for the entire period between March 10 and March 24. The color-coded circles show the ice + snow thickness [m] as measured with ALS (60 s average) and HEM (50 s average). The red cross indicates the position 77.9°N, 29.7°E of RV Lance at 15:00.

differences in the nadir brightness temperatures. The reason for the 10 K bias remains therefore speculative and restrains the use of the EMIRAD-2 nadir brightness temperatures in terms of absolute values.

5. SMOS ice thickness retrievals

For the following comparison we use two SMOS sea ice products of the University of Hamburg (UH) and University of Bremen (UB). Both products have been obtained from the respective websites, and no modifications have been applied. Thus, they represent the retrieval algorithms as described in Tian-Kunze et al. (2014) and Huntemann et al. (2014). The sea ice thickness products were derived from SMOS data based on the baseline processor version 505 operational in March 2014.

We calculate the temporal average of all SEM, HEM, and ALS measurements over the period of March 18 to 27 in order to achieve sufficient spatial coverage. We acknowledge that the UH SMOS thickness is already corrected for a statistical thickness distribution and should therefore be compared to the mean and not the modal ice thickness. The data are spatially averaged using the arithmetic mean value of all measurements within grid cells of 12.5 km resolution (same as the UH SMOS product grids) without any weighting. The resulting average gridded mean is first calculated separately for the different sensors and in a second step combined in a single thickness field which is taken for validation of the satellite data. We thereby assume that the average compensates to some extent preferential sampling biases

inherent in the different data sets: the shipborne measurements probably underestimate the ice thickess due to local navigation through leads and the limited ice-breaking capability up to about 0.5 m while the helicopter was not flying over open water and thin ice due to safety reasons. The SMOS thicknesses are temporally averaged over a slightly shortened period as the ground data. March 18 and 27 are not considered because of the sparse data coverage with only SEM data on this two days. An analysis performed for the single days of SMOS data (not shown) yields similar statistical parameters not significantly different compared to those numbers discussed in the following with the only exception of March 24.

The spatial distribution of the ground data together with the SMOS ice thickness (UH product) is shown in Fig. 7. It should be noted that the UB thickness product (not shown) resembles the spatial patterns but resolves ice thickness only up to a maximum of 0.5 m (thus, a retrieved thickness of 0.5 m means thickness ≥0.5 m). The statistical parameters of the comparisons are summarized in Table 2.

The overall linear correlation coefficient between the combined ground data and the two different SMOS thickness products is $R = 0.75$. The day with the highest in-situ gradient, March 24 with tracks including the patch of thick deformed ice, shows a higher correlation coefficient of about $R \approx 0.9$ (Fig. 8). Other days with a smaller gradient show smaller correlations.

Both SMOS data products underestimate the thickness on average by about 50–60%. However, the UH product performs better in comparison
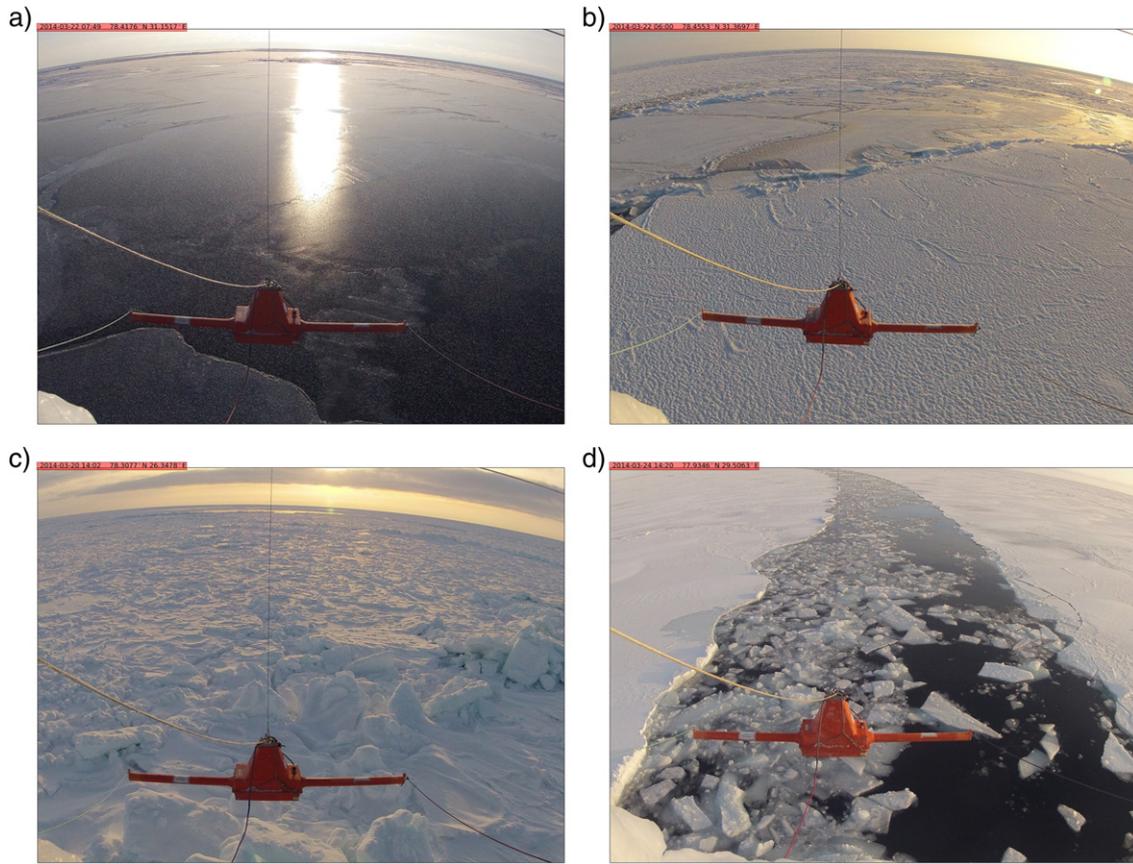
Fig. 4. Example ice conditions and EM thicknesses measured at the bow of RV Lance: a) Dark nilas of 2–4 cm thickness, b) grey white level ice of 17 cm thickness, c) pressure/rubble ice field of 3.4 m thickness, d) navigating through a lead with a mean thickness of 17 cm.

with the UB product with a reduced mean difference and RMSD. When the SMOS products are compared only against the SEM data they both agree within 1 cm with an observed mean thickness of 17 cm along the ship track of Lance. However, Lance is not an ice-breaker and its ability to navigate through the ice is limited to relatively thin ice to up to about half a meter level ice thickness. Pressure ridges appear on a very local scale and frequently resulted in an interruption of the route validation. The validation is further complicated because of the manual optimization by the helmsmen who preferably navigated through

open leads (Fig. 4d). The very local navigation and the different location of the thickness transects is a likely cause for the mean difference between the (thicker) airborne ALS and HEM data in comparison to the (thinner) HEM measurements. The SEM measurements are neither correlated to HEM or ALS nor to SMOS thickness data. However, the SEM instrument provided accurate thickness measurements which were in very good agreement with visual estimates of the level ice thickness.

Fig. 8 shows the thickness distribution and a scatter plot for the case of March 24. The combined airborne (ALS and HEM) data reveal a
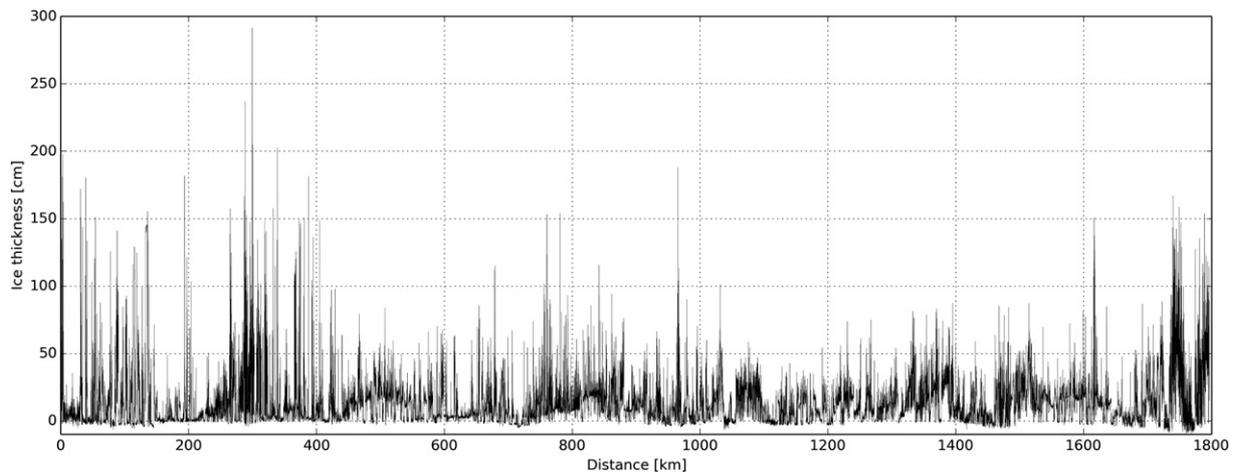

Fig. 5. Sea ice thickness profile measured with the SEM at the bow of RV Lance from March 18 to 27, 2014. The location of the 1800 km long track is shown in Fig. 7. The thickness measurements were spatially averaged over 25 m distances according to the GPS position of RV Lance.
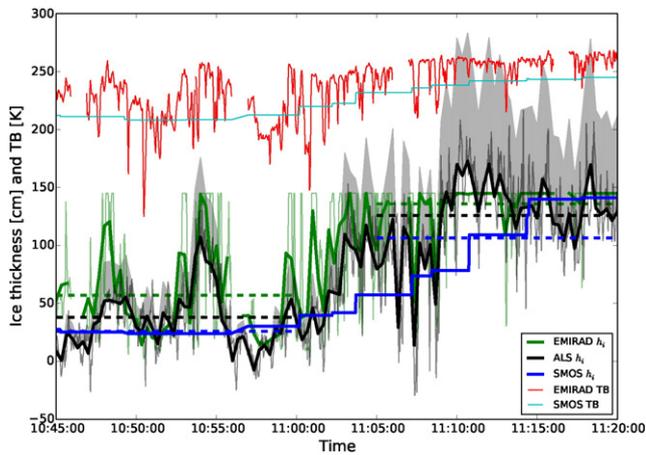
Fig. 6. Sea ice thickness derived from ALS surface elevation and EMIRAD-2 brightness temperature (TB) on March 24, 2014. The thin and thick lines represent 2 s and 20 s averages, respectively. The TB is averaged along track and the freeboard is averaged along and across-track for ALS. EMIRAD-2 measured TB near nadir while the SMOS TB is the average between nadir and 40° taken from the closest grid cells. The values for the ice thickness from SMOS were taken from the UH product and the same algorithm was used to derive the ice thickness from EMIRAD-2 TB. The thick black line indicates the sea ice thickness derived with the assumption of $h_s = 0.1 \cdot h_i$ while the upper limit of the grey shaded area is calculated without snow. The dashed lines indicate the mean values when only the first and last 15 min are considered.

Fig. 8. Sea ice thickness distributions and scatter plot for the case of March 24. The histograms and probability distribution functions (PDF) were derived from the gridded HEM and ALS validation data. The corresponding flight tracks are shown in Fig. 3. The SMOS histogram and the scatter plot was derived from the corresponding pixels of the ground data (number of pixels $N = 32$). The error bars in the scatter plot show the uncertainty as provided with the UH product. The solid lines are lognormal PDFs. A linear regression (inset) yields $Y = 0.71 * X - 0.01$ [m] with a correlation $R = 0.88$. The mean and standard deviation are $\mu_G \pm \sigma_G = 0.79 \pm 0.5$ m for the airborne ground data (ALS and HEM average) and $\mu_S \pm \sigma_S = 0.55 \pm 0.4$ m for SMOS. The mean and RMS difference are 0.24 m and 0.34 m, respectively.

bi-modal distribution in the thickness histogram. SMOS and airborne data agree well over the thin ice with a modal thickness of about 20 cm. The thicker deformed ice is substantially underestimated in the SMOS product resulting in a mean thickness difference of about 30%. The correlation $R = 0.88$ between SMOS and the airborne data is similar to the correlation between EMIRAD-2 and ALS shown in the previous section.

6. Forecast model and ship-route optimization

This section describes the application of SMOS data for the initialisation of forecast models. SMOS sea ice thickness is only one data source among others that are fed into the model system. A model system as described below allows the combination of different data sources to derive new information and physical quantities, like sea ice drift and convergence, and to provide a physically-consistent spatio-temporal interpolation and forecast.
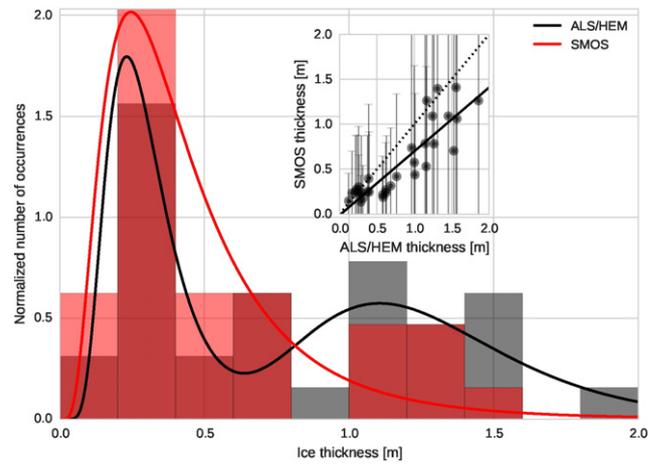
The model system consists of two components: First, the Arctic-wide variational assimilation system ICEDAS, which is based on the coupled ocean-sea ice model NAOSIM (North Atlantic/Arctic Ocean–Sea–Ice Model) developed at the AWI (Gerdes, Karcher, Kauker, & Schauer, 2003). ICEDAS generates an optimized ocean–sea–ice state estimate and a 7 day forecast on a grid with 0.5° horizontal resolution. This model is used to assimilate the SMOS sea ice thickness and AMSR2 ice concentration (both UH products) and the snow thickness derived from AMSR2 (UB product) together with the sea surface temperatures from AVHRR (OSI SAF high latitude SST product).

The forecasts of ICEDAS are then used as boundary and initial values for the nested, regional model system HAMMER (Hamburg System for Mesoscale ice forecast and Route optimization). HAMMER consists of coupled models for sea ice, atmosphere, and ocean, namely MESIM (Birnbaum, 1998; Dierer, Schlünzen, Birnbaum, Brümmer, & Müller, 2005; Schlünzen et al., 2012), METRAS (Schlünzen, 1990), and HAMSOM (Backhaus, 1985; Pohlmann, 1996, 2006). Additional
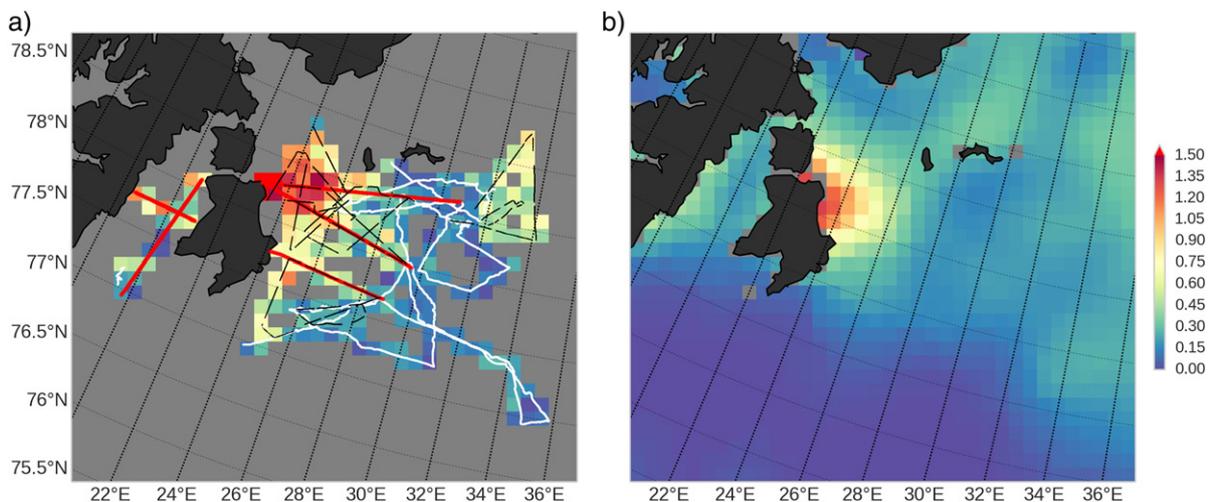

Fig. 7. Ground (left) and SMOS sea ice thickness (right) color-coded in meter. The ground data consists of SEM (white) and HEM (black) and ALS (red) measurements block averaged with 12.5 km grid resolution. The SMOS map represents a temporal average over the period March 19 to 26.
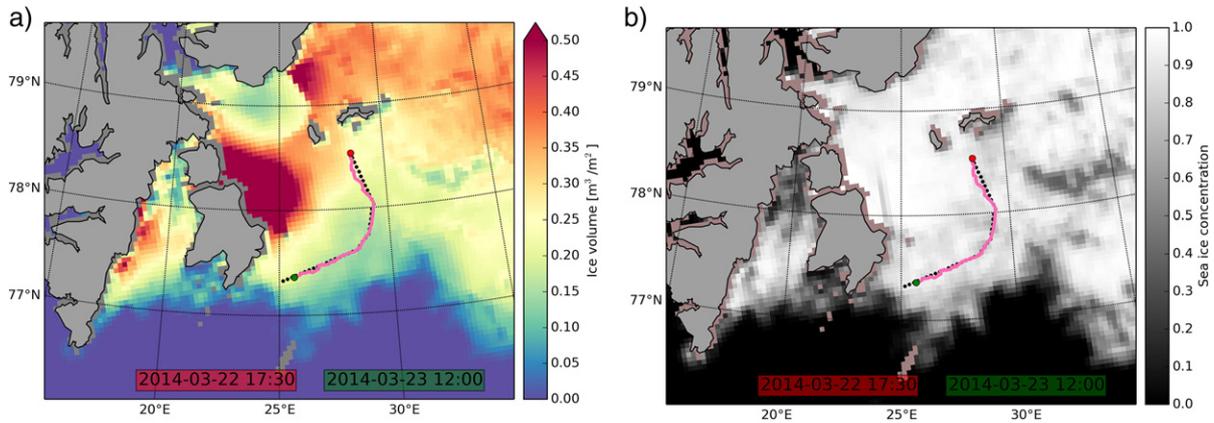
Fig. 9. Example of optimized route suggestion from the forecast system (black dotted line) and actual track of RV Lance (magenta line) overlaid on sea ice thickness (left) and concentration (right) from the forecast model. The mean sea ice thickness per grid cell is the product from the model effective sea ice thickness h_i and concentration C which equals the sea ice volume per unit area.

boundary values for the ocean are provided by the tidal model FES2004 (Lyard, Lefevre, Letellier, & Francis, 2006). Both systems, the coarse resolution ICEDAS and the nested higher resolution HAMMER, are forced by the global weather forecast provided by the European Centre for Medium-Range Weather Forecasts (ECMWF, 2014). A 830 km × 1125 km wide area between Svalbard and Franz–Josef Land was defined as the HAMMER spatial model domain with a horizontal grid resolution of 5 km. HAMMER sea ice forecasts are started twice daily, initialized with a combination of ICEDAS forecasts, SMOS ice thickness, and high resolution (3 km) AMSR2 ice concentrations (Beitsch, Kaleschke, & Kern, 2014) from the previous days.

Each HAMMER ice forecast covers 138 h. Predicted ice parameters were used for the routing software ICEROUTE to calculate an optimized route suggestion depending on the specific ship parameters (Reimer, 2015). The forecast and route optimization system was tested with RV Lance during the operational test phase in March 2014. Fig. 9 shows an example of a route suggestion together with its validation track on March 22/23. In this case the predicted travel time deviated from the actual time by about 18%, the route took 17.5 h instead of the predicted 15 h. In total 12 route suggestions have been tested during the field experiment while the length of each route was restricted by the limiting ice conditions for operated ship RV Lance. In most cases the boundary lines between two different ice classes in terms of thickness and concentration were predicted well by the forecast sytsem. The routes could therefore be adapted along these boundary lines to optimize the travel time by preventing continuous progress of the ship and minimizing the distance. The average speed of the ship could not be predicted with very high accuracy by the system as the ice forecast was not resolving very local variations in ice parameters relevant for short range routing. A quantitative hindcast assessment of the skill was performed in terms of threat indices, which indicate if the forecasts correctly state whether a route is navigable or not. It was demonstrated that the system is able to reduce danger for ships because it forecasts non-navigable routes better than assuming persistence of the ice conditions (Gierisch, 2015).

7. Conclusion

A comprehensive validation field campaign in the Barents Sea was conducted in March 2014. An anomalously strong ice retreat together with the subsequent refreezing was perfectly suited to obtain sea ice thickness validation data over relatively thin ice in the seasonal ice zone. Measurements from the ice strengthened research vessel Lance, a helicopter based on Lance, and the research aircraft Polar 5 operated from Svalbard airport form an extensive and unique sea ice thickness validation data set. High resolution brightness temperatures were measured with the EMIRAD-2 L-band radiometer aboard the Polar 5. This ground data was used for a comparison to SMOS-based estimates of the sea ice thickness. Furthermore, the results from the forecast model were used for the application of a ship route optimization system. The salient points of the comparisons are revisited in the following.

The overall main pattern of the spatial thickness distribution is well captured in two different SMOS sea ice products from the Universities of Hamburg (UH) and Bremen (UB). The origin of a patch of thick deformed ice at the east coast of EdgeÃ¸ya was determined using

Table 1
Primary thickness validation datasets.

Platform	Sensors	Periods	Comments
RV Lance	SEM, KT19	18. 15:19–27. 11:09	Fig. 5
Polar 5	ALS, EMIRAD-2	24. 9:15–12:52	Figs. 3 and 6
		26. 8:47–12:22	
		26. 14:27–16:27	CryoSat underflight
Helicopter	HEM	19. 14:50–15:42	
		20. 08:52–11:03	CryoSat underflight
		20. 14:23–16:28	CryoSat underflight
		22. 08:32–10:52	
		22. 13:51–15:55	
		23. 12:45–13:56	
		24. 10:39–13:16	Figs. 3 and 6
		26. 11:06–13:17	With Polar-5

Table 2
Statistical comparison between SMOS and ground sea ice thickness for different subsets (selected pixels with 12.5 km resolution) averaged over the entire spatial and temporal domain. The subsets are selected according to different data sources and conditions. The ground (index G) and SMOS (index S) thickness mean and standard deviation for different subsets are given in the second and third column, respectively. Measurements and SMOS data have been averaged as described in Section 4. Correlation R, mean difference (MD), and root mean square difference (RMSD) have been calculated on pixel level. The number of pixel data pairs is given in the fourth column. The condition based on the UB product ($h_{UB} < 0.5$ m) results in $N = 213$ selected pixels with the UB SMOS ice thickness below half a meter. This subset of pixels is also for the UH product to derive a consistent comparison. The two first rows refer to the comparison of the UH and UB SMOS product for the entire averaged ground data (SEM&HEM&ALS), respectively. All units are in [cm] except for correlations and number of pixels N.

Data	$\mu_G \pm \sigma_G$	$\mu_S \pm \sigma_S$	N	R	MD	RMSD
SMOS UH	44 ± 36	26 ± 19	229	0.75	−18	31
$h_{UB} < 0.5$ m	39 ± 30	22 ± 10	213	0.65	−15	29
SEM	17 ± 13	18 ± 7	121	0.12	−1	14
HEM&ALS	65 ± 33	31 ± 21	149	0.72	−33	41
SMOS UB	44 ± 36	22 ± 11	229	0.76	−22	36
$h_{UB} < 0.5$ m	39 ± 30	19 ± 8	213	0.66	−20	32
SEM	17 ± 13	17 ± 5	121	0.10	0	14
HEM&ALS	65 ± 33	25 ± 12	149	0.70	−40	48

272 *L. Kaleschke et al. / Remote Sensing of Environment 180 (2016) 264–273*

trajectories of ice drift buoys that were deployed before the field campaign. The upper value of the thickness range was set by this area of deformed ice with thickness between 1 and 3 m. The lower range was determined by an area of newly formed sea ice with a mean thickness of 17 cm that was extensively sampled by the shipborne EM on Lance. The thickness gradient between the new thin ice and the thick ice is well represented by the airborne sensors as well as with the SMOS products. The SMOS retrieval substantially underestimates the thickness of the deformed thick ice but agrees well with the shipborne measurements in the extensive areas of newly grown young sea ice.

The UB SMOS product provides ice thickness only up to a maximum of 0.5 m while the UH product resolves thicknesses up to about 1.5 m. Sea ice thickness derived from high resolution EMIRAD-2 data using the UH SMOS retrieval algorithm mostly agrees with the thickness derived from the airborne laser scanner within the range of uncertainties and shows correlations up to 1.5 m. A statistical bias correction had to be applied to the EMIRAD-2 nadir data because of contamination with radio frequency interference (RFI) from a camera. Another large uncertainty is caused by the insufficient knowledge about the snow thickness. A new snow radar system aboard the Polar 5 did not perform as expected and the data could not be used for the analysis. We recommend further validation campaigns with an improved snow radar to close this gap of knowledge.

The validity and usefulness of the sea ice forecast and ice route optimization system have been exemplified. The model system allows a physically-consistent interpolation and a forecast providing added-value data products. However, the average speed of the ship could not be predicted with very high accuracy because the forecast was not resolving very local ice variations relevant for short range routing. The local occurrence of thick ice and ridges restricted the operation of RV Lance and limited the length of the in total 12 route suggestions tested during the field experiment.

We conclude that the SMOS sea ice thickness product was very useful in the framework of the operational sea ice forecast system but further improvements of the SMOS retrieval algorithm are necessary in particular over deformed ice areas. The synergistic combination of SMOS and the CryoSat2 altimeter may be a possible alternative to cover the full thickness range (Kaleschke et al., 2015). Insufficient knowledge about the snow cover remains as the most challenging uncertainty.

Acknowledgements

The IRO2 project and in particular the trial with RV Lance was a nucleus for an extensive field experiment with other national and international participation and co-funding. IRO2 was funded by the Federal Ministry for Economic Affairs and Energy (BMWi) under the contract 03SX328A (PI P. Jochmann). RV Lance was chartered for the period 14/3-29/3-2014 by the University of Hamburg (PI L. Kaleschke). The European Space Agency co-financed the AWI research aircraft Polar 5 and helicopter flights (ESA contract 4000110477/14/NL/FF/lf; PI S. Hendricks) and the development and validation of SMOS sea ice thickness retrieval methods (ESA contracts 4000101476/10/NL/CT and 4000112022/14/I-AM; PI L. Kaleschke). Norwegian Polar Institute co-financed and conducted the helicopter measurements with the EM-bird. Technical University of Denmark (DTU) co-financed and conducted the measurements with EMIRAD-2 L-band radiometer on Polar 5. The German Aerospace Center (DLR) provided Terra-SAR-X data under the science proposal IDs OCE1891 and OCE2192 (PI. L. Kaleschke). Cosmo-Skymed images were provided over an *e*-GEOS project (PI J. Holfort). Procurement and application of CALIB-I drift buoys from Metocean (Canada) through DFG (EXC177, PI. L. Kaleschke). Funding of the project CORESAT by the Research Council of Norway (project 222681) is acknowledged. S. Hendricks was funded by the German Ministry of Economics and Technology (Grant 50EE1008). ECMWF and the German Meteorological Service DWD are acknowledged for providing meteorological forecasts and data for testing the operational application of the IRO system including all the forecast models. ICEDAS was developed and operated by Frank Kauker, Thomas Kaminski, and Jochen Segschneider, who also provided highly valuable comments on this manuscript. We also thank the crews of RV Lance and Airlift helicopter and the technicians and engineers Marius Bratrein, Martin Schiller, and Michael Offermann for their great effort during the campaign.

References

Backhaus, J. O. (1985). A Three-Dimensional Model for the simulation of shelf sea dynamics. *Deutsche Hydrografische Zeitschrift*, 38, 165–187. http://dx.doi.org/10.1007/BF02328975.

Beitsch, A., Kaleschke, L., & Kern, S. (2014). Investigating high-resolution AMSR2 sea ice concentrations during the February 2013 Fracture Event in the Beaufort Sea. *Remote Sensing*, 6, 3841–3856. http://dx.doi.org/10.3390/rs6053841 (URL: http://www.mdpi.com/2072-4292/6/5/3841).

Birnbaum, G. (1998). Numerische Modellierung der Wechselwirkung zwischen Atmosphäre und Meereis in der arktischen Eisrandzone = Numerical modelling of the interaction between atmosphere and sea ice in the Arctic marginal ice zone. *Berichte zur Polarforschung (Reports on Polar Research)*, 268 (176 pp. URL: http://hdl.handle.net/10013/epic.10271).

Day, J. J., Hawkins, E., & Tietsche, S. (2014). Will arctic sea ice thickness initialization improve seasonal forecast skill? *Geophysical Research Letters*, 41, 7566–7575. http://dx.doi.org/10.1002/2014GL061694 (URL: http://dx.doi.org/10.1002/2014GL061694).

Dierer, S., Schlünzen, K. H., Birnbaum, G., Brümmer, B., & Müller, G. (2005). Atmosphere–sea–ice interactions during a cyclone passage investigated by using model simulations and measurements. *Monthly Weather Review*, 133, 3678–3680. http://dx.doi.org/10.1175/MWR3076.1.

Dobrynin, M., & Pohlmann, T. (2015). Anomalous hydrographic conditions in the western Barents Sea observed in march 2014. *Continental Shelf Research*, 111(Part A), 69–82. http://dx.doi.org/10.1016/j.csr.2015.10.020 (URL: http://www.sciencedirect.com/science/article/pii/S0278343415300959).

ECMWF (2014). IFS Documentation – Cy40r1. *Operational implementation 22 November 2013* (URL: http://www.ecmwf.int/en/forecasts/datasets/dataset-i-i-atmospheric-fields-high-resolution-forecast. published by the European Centre for Medium-Range Weather Forecasts (ECMWF) at http://old.ecmwf.int/research/ifsdocs/CY40r1/index.html, accessed on 06/06/2014).

Gerdes, R., Karcher, M. J., Kauker, F., & Schauer, U. (2003). Causes and development of repeated Arctic Ocean warming events. *Geophysical Research Letters*, 30. http://dx.doi.org/10.1029/2003GL018080 (1980, n/a–n/a. URL: http://dx.doi.org/10.1029/2003GL018080).

Gierisch, A. M. U. (2015). *Short-range sea ice forecast with a regional coupled sea–ice–atmosphere–ocean model.* (Ph.D. thesis) Hamburg: Staats- und Universitätsbibliothek Hamburg (URL: http://ediss.sub.uni-hamburg.de/volltexte/2015/7477).

Haas, C. (1998). Evaluation of ship-based electromagnetic-inductive thickness measurements of summer sea-ice in the Bellingshausen and Amundsen Seas, Antarctica. *Cold Regions Science and Technology*, 27, 1–16. http://dx.doi.org/10.1016/S0165-232X(97)00019-0 (URL: http://www.sciencedirect.com/science/article/pii/S0165232X97000190).

Haas, C., Lobach, J., Hendricks, S., Rabenstein, L., & Pfaffling, A. (2009). Helicopter-borne measurements of sea ice thickness, using a small and lightweight, digital em system. *Journal of Applied Geophysics*, 67, 234–241. http://dx.doi.org/10.1016/j.jappgeo.2008.05.005 (airborne Geophysics, URL: http://www.sciencedirect.com/science/article/pii/S0926985108000682).

Helm, V., Hendricks, S., Göbell, S., Rack, W., Haas, C., Nixdorf, U., & Boebel, T. (2006). *Cryovex 2004 and 2005 (bob) data acquisition and final report.* Bremerhaven, Germany: Alfred Wegener Institute.

Hendricks, S., Steinhage, D., Helm, V., Birnbaum, G., Skou, N., Kristensen, S. S., ... Kaleschke, L. (2014). SMOSice 2014: Data acquisition report. URL: https://earth.esa.int/web/guest/campaigns Project: Technical support for the 2014 SMOSice campaign in SE Svalbard ESA contract number: 4000110477/14/NL/FF/lf technical report No. 1, 2014.

Huntemann, M., Heygster, G., Kaleschke, L., Krumpen, T., Mäkynen, M., & Drusch, M. (2014). Empirical sea ice thickness retrieval during the freeze-up period from SMOS high incident angle observations. *The Cryosphere*, 8, 439–451. http://dx.doi.org/10.5194/tc-8-439-2014 (URL: http://www.the-cryosphere.net/8/439/2014/).

Kaleschke, L., Maass, N., Haas, C., Heygster, S., & Tonboe, R. (2010). A sea ice thickness retrieval model for 1.4 GHz radiometry and application to airborne measurements over low salinity sea ice. *The Cryosphere*, 4, 583–592. http://dx.doi.org/10.5194/tc-4-583-2010.

Kaleschke, L., Tian-Kunze, X., Maas, N., Ricker, R., Hendricks, S., & Drusch, M. (2015). Improved retrieval of sea ice thickness from smos and cryosat-2. *Geoscience and Remote Sensing Symposium (IGARSS), 2015 IEEE International* (pp. 5232–5235). http://dx.doi.org/10.1109/IGARSS.2015.7327014.

Kaleschke, L., Tian-Kunze, X., Maaß, N., Heygster, G., Huntemann, M., Wang, H., ... Haas, C. (2013). SMOS sea ice retrieval study (SMOSIce), ESA support to science element (STSE). *Final report ESA ESTEC contract no.: 4000101476/10/NL/CT.* Univ. Hamburg, Institute of Oceanography (380 pages).

Kaleschke, L., Tian-Kunze, X., Maaß, N., Mäkynen, M., & Drusch, M. (2012). Sea ice thickness retrieval from SMOS brightness temperatures during the Arctic freeze-up period. *Geophysical Research Letters*, 39. http://dx.doi.org/10.129/2012GL050916.

Kerr, Y. H., Waldteufel, P., Wigneron, J. P., Martinuzzi, J., Font, J., & Berger, M. (2001). Soil moisture retrieval from space: The Soil Moisture and Ocean Salinity (SMOS) mission. *IEEE Transactions on Geoscience and Remote Sensing, 39*, 1729–1735. http://dx.doi.org/10.1109/36.942551.

Kwok, R., & Cunningham, G. F. (2015). Variability of Arctic Sea ice thickness and volume from CryoSat-2. *Philosophical Transactions of the Royal Society of London A: Mathematical, Physical and Engineering Sciences, 373*. http://dx.doi.org/10.1098/rsta.2014.0157.

Laxon, S. W., Giles, K. A., Ridout, A. L., Wingham, D. J., Willatt, R., Cullen, R., ... Davidson, M. (2013). Cryosat-2 estimates of Arctic sea ice thickness and volume. *Geophysical Research Letters, 40*, 732–737. http://dx.doi.org/10.1002/grl.50193 (URL: http://dx.doi.org/10.1002/grl.50193).

Lyard, F., Lefevre, F., Letellier, T., & Francis, O. (2006). Modelling the global ocean tides: Modern insights from FES2004. *Ocean Dynamics, 56*, 394–415. http://dx.doi.org/10.1007/s10236-006-0086-x (URL: http://dx.doi.org/10.1007/s10236-006-0086-x).

Maaß, N., Kaleschke, L., Tian-Kunze, X., Mäkynen, M., Drusch, M., Krumpen, T., ... Haas, C. (2015). Validation of SMOS sea ice thickness retrieval in the northern Baltic Sea. *Tellus A, 67*. http://dx.doi.org/10.3402/tellusa.v67.24617.

Mäkynen, M., Cheng, B., & Similä, M. (2013). On the accuracy of thin-ice thickness retrieval using modis thermal imagery over arctic first-year ice. *Annals of Glaciology, 54*, 87–96. http://dx.doi.org/10.3189/2013AoG62A166 (URL: http://www.ingentaconnect.com/content/igsoc/agl/2013/00000054/00000062/art00013).

Markus, T., & Cavalieri, D. J. (2013). *Snow depth distribution over sea ice in the southern ocean from satellite passive microwave data.* American Geophysical Union, 19–39. http://dx.doi.org/10.1029/AR074p0019 (URL: http://dx.doi.org/10.1029/AR074p0019).

Mecklenburg, S., Drusch, M., Kaleschke, L., Rodriguez-Fernandez, N., Reul, N., Kerr, Y., ... Kornberg, M. (2016). ESA's soil moisture and ocean salinity mission: From science to operational applications. *Remote Sensing of Environment.* http://dx.doi.org/10.1016/j.rse.2015.12.025 (URL: http://www.sciencedirect.com/science/article/pii/S0034425715302467).

Pavlova, O., Pavlov, V., & Gerland, S. (2014). The impact of winds and sea surface temperatures on the Barents Sea extent, a statistical approach. *Journal of Marine Systems, 130*, 248–255. http://dx.doi.org/10.1016/j.jmarsys.2013.02.011 (URL: http://www.sciencedirect.com/science/article/pii/S0924796313000456).

Pohlmann, T. (1996). Predicting the thermocline in a circulation model of the north sea – Part I: Model description, calibration and verification. *Continental Shelf Research, 16*, 131–146 (URL: http://www.sciencedirect.com/science/article/pii/027843439590885S).

Pohlmann, T. (2006). A *meso*-scale model of the central and southern north sea: Consequences of an improved resolution. *Continental Shelf Research, 26*, 2367–2385 (URL: http://www.sciencedirect.com/science/article/pii/S0278434306002123).

Reimer, N. (2015). Ship trial for testing an ice route optimization system. *OTC Arctic Technology Conference, 23–25 March, Copenhagen, Denmark.* http://dx.doi.org/10.4043/25601-MS.

Ricker, R., Hendricks, S., Helm, V., Skourup, H., & Davidson, M. (2014). Sensitivity of CryoSat-2 Arctic sea–ice freeboard and thickness on radar-waveform interpretation. *The Cryosphere, 8*, 1607–1622. http://dx.doi.org/10.5194/tc-8-1607-2014 (URL: http://www.the-cryosphere.net/8/1607/2014/).

Sandven, S., Johannessen, O. M., Miles, M. W., Pettersson, L. H., & Kloster, K. (1999). Barents Sea seasonal ice zone features and processes from ERS 1 synthetic aperture radar: Seasonal Ice Zone Experiment 1992. *Journal of Geophysical Research: Oceans, 104*, 15843–15857. http://dx.doi.org/10.1029/1998JC900050 (URL: http://dx.doi.org/10.1029/1998JC900050).

Schlünzen, K. H. (1990). Numerical studies on the inland penetration of sea breeze fronts at a coastline with tidally flooded mudflats. *Contributions to Atmospheric Physics, 63*, 243–248.

Schlünzen, K. H., Flagg, D. D., Fock, B. H., Gierisch, A., Lüpkes, C., Reinhardt, V., & Spensberger, C. (2012). Scientific documentation of the multiscale model system *M-SYS* (METRAS, MITRAS, MECTM, MICTM, MESIM). *MEMI technical report 4.* Meteorologisches Institut KlimaCampus, Universität Hamburg (138 pp. https://goo.gl/xv74Bi).

Smedsrud, L. H., Esau, I., Ingvaldsen, R. B., Eldevik, T., Haugan, P. M., Li, C., ... Sorokina, S. A. (2013). The role of the Barents Sea in the arctic climate system. *Reviews of Geophysics, 51*, 415–449. http://dx.doi.org/10.1002/rog.20017 (URL: http://dx.doi.org/10.1002/rog.20017).

Sobjaerg, S., Kristensen, S., Balling, J., & Skou, N. (2013). The airborne EMIRAD L-band radiometer system. *Geoscience and Remote Sensing Symposium (IGARSS), 2013 IEEE International* (pp. 1900–1903). http://dx.doi.org/10.1109/IGARSS.2013.6723175.

Strübing, K., & Schwarz, J. (2014). Die Eisverhältnisse in der Barentssee während der IRO-2-Testfahrt mit R/V Lance 17. – 27.03.2014. *Abschlussbericht vorgelegt von JS Consulting, Großhansdorf, im Auftrag des AWI; Bestellnummer 12/45086354 zum Werkvertrag Vor —/Nachbereitung und Durchführung der IRO-2-Testfahrt im Rahmen des Vorhabens Entwicklung und Optimierung eines Ozean-Meereis Vorhersagemodells für das Nordpolarmeer, BMWi-Förderkennzeichen: 03SX328H.*

Tian-Kunze, X., Kaleschke, L., Maaß, N., Mäkynen, M., Serra, N., Drusch, M., & Krumpen, T. (2014). SMOS-derived thin sea ice thickness: Algorithm baseline, product specifications and initial verification. *The Cryosphere, 8*, 997–1018. http://dx.doi.org/10.5194/tc-8-997-2014 (URL: http://www.the-cryosphere.net/8/997/2014/).

Warren, S. G., Rigor, I. G., Untersteiner, N., Radionov, V. F., Bryazgin, N. N., Aleksandrov, Y. I., & Colony, R. (1999). Snow depth on arctic sea ice. *Journal of Climate, 12*, 1814–1829.

Yang, Q., Losa, S. N., Losch, M., Tian-Kunze, X., Nerger, L., Liu, J., ... Zhang, Z. (2014). Assimilating SMOS sea ice thickness into a coupled ice–ocean model using a local seik filter. *Journal of Geophysical Research: Oceans, 119*, 6680–6692. http://dx.doi.org/10.1002/2014JC009963 (URL: http://dx.doi.org/10.1002/2014JC009963).

Yu, Y., & Rothrock, D. (1996). Thin ice thickness from satellite thermal imagery. *Journal of Geophysical Research-Oceans, 101*, 25753–25766.